9

Metal Oxide Nanowires – Structural and Mechanical Properties

L. Dai, C.H. Sow, C.T. Lim and V.B.C. Tan
National University of Singapore
Singapore

1. Introduction

Metal Oxide nanowires are versatile nanostructured materials with diverse yet unique properties. Potentially, they have a wide range of applications in electrical, chemical and semiconductor technologies (Yang, Wu et al. 2002; Rao, Deepak et al. 2003; Law, Goldberger et al. 2004; Shankar and Raychaudhuri 2005; Lu, Chang et al. 2006; Lu and Lieber 2006).

Research interests in metal oxide nanowires commenced in 1990s. Up to now, there have been a considerable number of reports on success in the synthesis of 1-dimensional nano-crystalline structured nanowires of various metal oxides, such as CuO(Wang, Zhan et al. 2001; Jiang, Herricks et al. 2002), MgO(Ma and Bando 2003), ZnO(Tian, Voigt et al. 2003; Vayssieres 2003; Heo, Norton et al. 2004; Wang, Song et al. 2007; Manoharan, Desai et al. 2008), TiO_2(Lakshmi, Partissi et al. 1997; Li and Wang 1999; Li and Xia 2003; Wu, Shih et al. 2005; Wu, Shih et al. 2006), Al_2O_3(Valcarcel, Souto et al. 1998; Xiao, Han et al. 2002), Ga_2O_3(Wu, Song et al. 2000), In_2O_3(Li, Zhang et al. 2003), SnO_2(Dai, Pan et al. 2001), Sb_2O_5(Guo, Wu et al. 2000), V_2O_5(Chen, Sun et al. 2002), $BaTiO_3$(Urban, Spanier et al. 2003), etc. The methodology of synthesis is now well developed. Reported techniques include vapor-solid phase technique(Valcarcel, Souto et al. 1998; Wu, Song et al. 2000; Jiang, Herricks et al. 2002; Ma and Bando 2003; Wu, Shih et al. 2005; Wu, Shih et al. 2006), chemical solution deposition (sol-gel) (Lakshmi, Partissi et al. 1997; Urban, Spanier et al. 2003), template etching(Xiao, Han et al. 2002), percipitation(Tian, Voigt et al. 2003; Vayssieres 2003), micro-emulsion(Guo, Wu et al. 2000), flux growth(Dai, Pan et al. 2001) and others. These are well reviewed by Shangkar et al.(Shankar and Raychaudhuri 2005).

Among all the properties of metal oxide nanowires, their mechanical property is one of the most highly structure dependent and features strongly in many applications. The structural and mechanical phenomena and related mechanisms have attracted significant research interests. However, due to the difficulties in manipulating the nano-sized specimens, experimental characterizations are limited to simple mechanical tests to measure quantities like Young's modulus, strength et al. Comparatively, numerical studies, especially molecular dynamics (MD) simulations, are well suited for nanostructured materials, and have been broadly applied for investigating structural and mechanical properties. In this chapter, we will review the structural characteristics and mechanical properties of different types of metal oxides, both experimentally and numerically. Besides reviewing published literatures, we will be focusing on reporting the outputs from our research group.

2. Metal oxide nanowires

2.1 ZnO

ZnO nanocrystals possess large energy bandgap and excitation binding energy, which ensures efficient excitonic emission at room temperature. This makes it a fascinating material in potential optoelectronic applications(Wang, Song et al. 2007). Their mechanical stability is a key factor for promising working conditions, and draws significant research interest.

Experimental measurements, such as bending resonance(Bai, Gao et al. 2003; Yum, Wang et al. 2004; Chen, Shi et al. 2006; Huang, Bai et al. 2006; Ni and Li 2006; Zhou, Lao et al. 2006), bending deflection(Song, Wang et al. 2005; Manoharan, Desai et al. 2008; Wen, Sader et al. 2008), nano-indentation(Feng, Nix et al. 2006; Ni and Li 2006) and tensile stretching(Desai and Haque 2007; Hoffmann, Ostlund et al. 2007; Agrawal, Peng et al. 2008) have been carried out to measure the Young's modulus ZnO. These results deviate significantly over a wide range from 20 to 220 GPa. The lack of agreement was considered to be due to differences in degree of crystallinity, direction of loading, boundary conditions, and sample manipulations, etc. Similar scatter was also seen in hardness and ultimate tensile strength (UTS), 2.5-4.3 GPa(Feng, Nix et al. 2006) and 2.5-7.5 GPa(Hoffmann, Ostlund et al. 2007; Wen, Sader et al. 2008), respectively.

In contrast to the abundant experimental characterizations, theoretical reports on the structure and mechanical property of ZnO nanowires have not been insightful. Kulkarni et al.(Kulkarni, Zhou et al. 2005) carried out tensile simulations on ZnO nanobelt with square cross sections. It was found that the structure transformed into multi-shell structure for wires thinner than 10Å, whereas thicker nanowires maintained a crystalline structure after equilibration. The decrease in Young's modulus and UTS with increasing nanowire thickness is attributed to the high compressive internal stress induced by the free surface of the wire In a later publication by the same group(Wang, Kulkarni et al. 2008), simulations of the wurtzite crystalline structured ZnO nanowires with hexagonal lateral geometry showed three stages of deformation when the wires were loaded in tension - wurtzite elastic stretch, phase transformation from wurtzite to body-centered-crystal (BCC) structure, and BCC elastic stretch. From the stress-strain curve, the Young's modulus was measured to be 227-299GPa for nanowires with thickness ranging from 45.5 to 19.5Å. These values are much higher than the bulk value of 140GPa. It is noted that the high stretch rate of 10-50m/s could have led to the exceptionally high stiffness and unexpectedly low toughness. In a recent literature, Agrawal et al.(Agrawal, Peng et al. 2008) reported values of 140-160GPa for the Young's modulus of 5-20Å thick [0001] oriented hexagonal ZnO nanowires, with thinner nanowires to be reportedly stiffer. The results are in agreement with bulk values and their experimental measurements.

We carried out MD simulations to model a tensile process on the ZnO nanowire at a moderate stretching rate. By presenting the structural deformation and mechanical response(Dai, Cheong et al. 2010), the mechanism behind observations were revealed.

We adopt the Buckingham potential with Kulkarni's parameters(Kulkarni, Zhou et al. 2005) to describe the atomic interactions. This potential successfully reproduces the ZnO crystalline lattice parameters. The cylindrical ZnO nanowires were built from super cells of wurtzite crystal with [0001] in the longitude direction. Atoms in the top and bottom five layers were prescribed to displace as two rigid blocks to stretch the wires while all other atoms were free of constraints. Free surface conditions were applied in all directions. The

molecular dynamics simulation was carried using the DL-POLY software (http://www.cse.scitech.ac.uk/ccg/software/DL_POLY/) with time steps of 2 fs. The temperature was maintained at 300 K by scaling the atomic velocities every 1 ps. The nanowires were firstly relaxed under constant atmosphere pressure (NPT) for 1 ns to remove internal stresses, and under constant volume (NVT) for another 1 ns to reach the minimum energy state. The tensile process was carried out via displacing the top and bottom blocks of atoms in a stepwise manner. For each step, the nanowire was stretched by 1Å and equilibrated for 500 ps, i.e., a tensile rate of 0.2 m/s. The total system energy and atomic positions were monitored to ensure the wires achieved equilibrium at the end of 500 ps. This methodology was used for all the tensile MD simulations in this chapter.

Four ZnO nanowires with lateral diameters of 7Å, 16Å, 25Å and 40Å were constructed. Their initially relaxed structures are shown in Fig.1. The thinnest 7Å nanowire experienced a structure transformation into a totally amorphous state, due to the strong surface effect. The degree of amorphization retarded with increase in lateral size. Complete crystalline structures

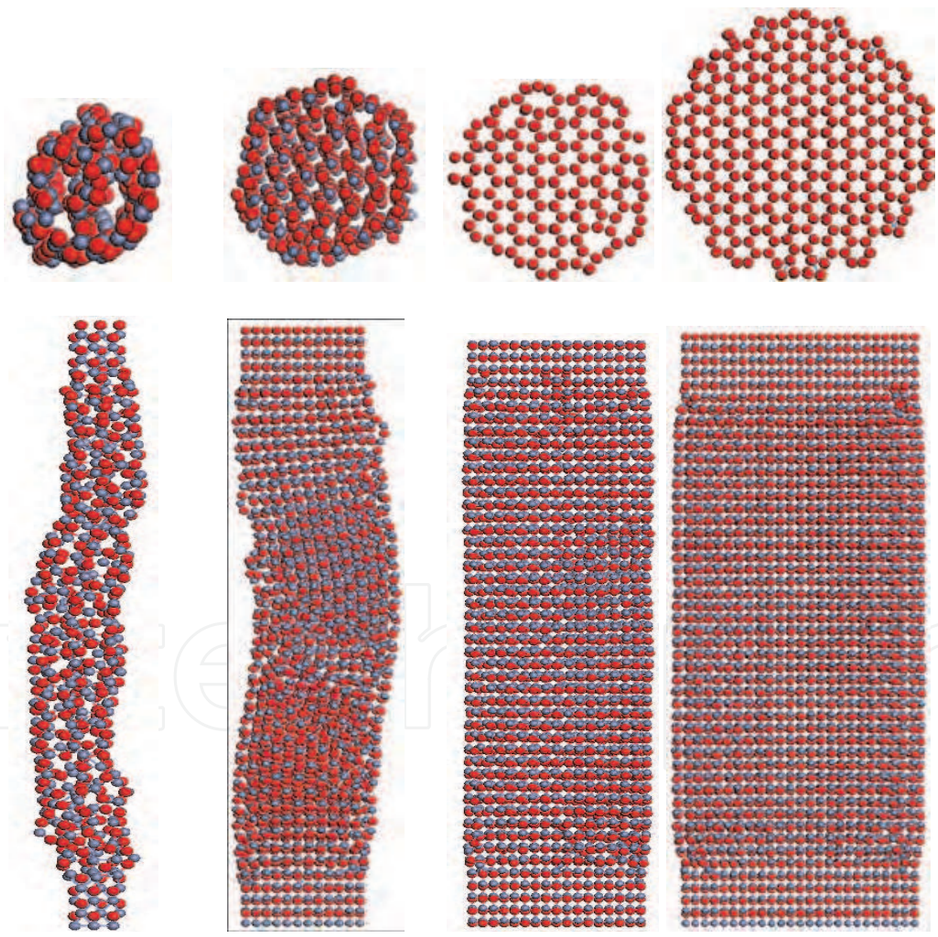

(a) (b) (c) (d)

Fig. 1. Equilibrated structure of ZnO nanowires with lateral diameters of (a) 7Å, (b) 16Å, (c) 25Å, and (d) 40Å. Cross-sectional views at the nanowire center are shown at the top. Red spheres denote O atoms and grey Zn atoms.

were retained for nanowires with lateral diameter 25Å and above. A 16Å nanowire was presented as the transient state between amorphous and crystalline state. The threshold diameter for crystalline to amorphous transformation was about the length of 3-4 single crystal lattices. This empirical observation is also applicable for many other inorganic materials, such as metals, semiconductors and ceramics, in agreement with previous reports for crystals of Au(Kondo and takayanagi 2000; Wang, Yin et al. 2001),Al(Gulseren, Ercolessi et al. 1998), Pb(Gulseren, Ercolessi et al. 1998), Ti(Wang, Yin et al. 2001), SiC(Maleev, Srivastava et al. 2006).

The snapshots of tensile process for nanowires are presented for the 7Å and 25Å nanowires in Fig. 2 and Fig.3, respectively. Under tensile loading, the 7Å nanowire firstly straightened (Fig.2b), and then necked at 35.6% strain (Fig.2c). Once formed, the necked region, where stress concentrated, thinned further to a single-atom-neck chain (Fig.2d). With further stretching, more atoms were continuously pulled into the single-atom-neck, resulting in a very ductile behavior (Fig.2e, f).

The 25Å nanowire presented a novel tensile deformation process as shown in Fig.4. Initially, the original crystals in the nanowire only experienced slight and homogeneous longitude stretching without significant phase transformations. At 12.5% strain (Fig.3a, b), ZnO bond breakage occurred and structural deformation was seen at the central section (Fig.3c). This region experienced high strain and propagated quickly to create a lateral slip-deformed necking (Fig.3d). With continued stretching, the tensile process followed a three-step cycle - 1) straightening of Zn-O bonds in the necked region, 2) neck thinning, 3) relaxation of the necked region as new atoms were pulled into the neck. The nanowire was able to be extremely ductile with the iteration of the three-step plastic deformation cycle.

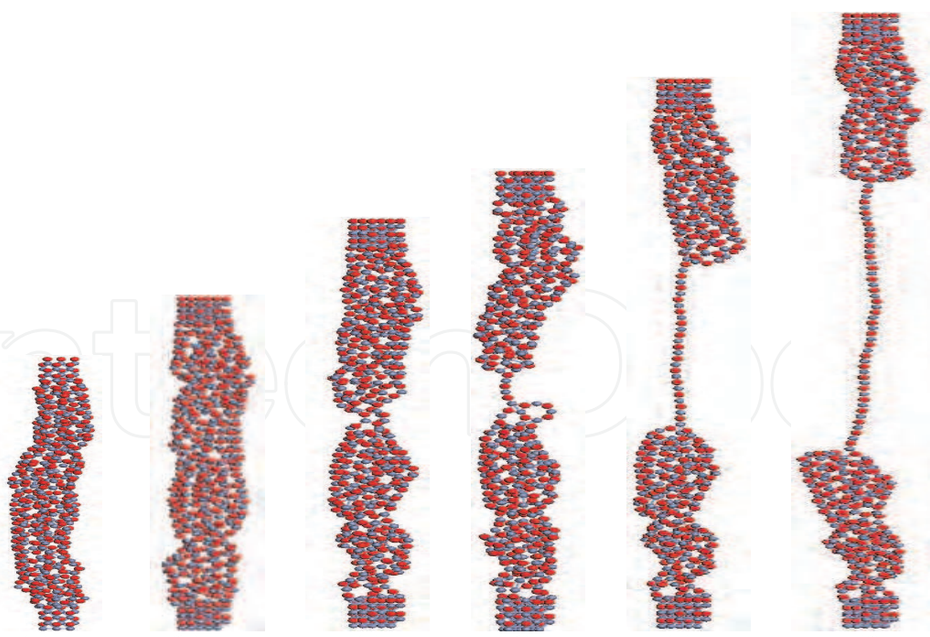

Fig. 2. Tensile stretching of 7Å diameter ZnO nanowire - (a) equilibration, (b) straightening at 16.5% strain, (c) initiation of necking at 35.6% strain, (d) formation of single-atom-neck at 41.9% strain, (e) continued growth of single-atom-neck at 77.5% strain, and (f) nanowire at 116% strain.

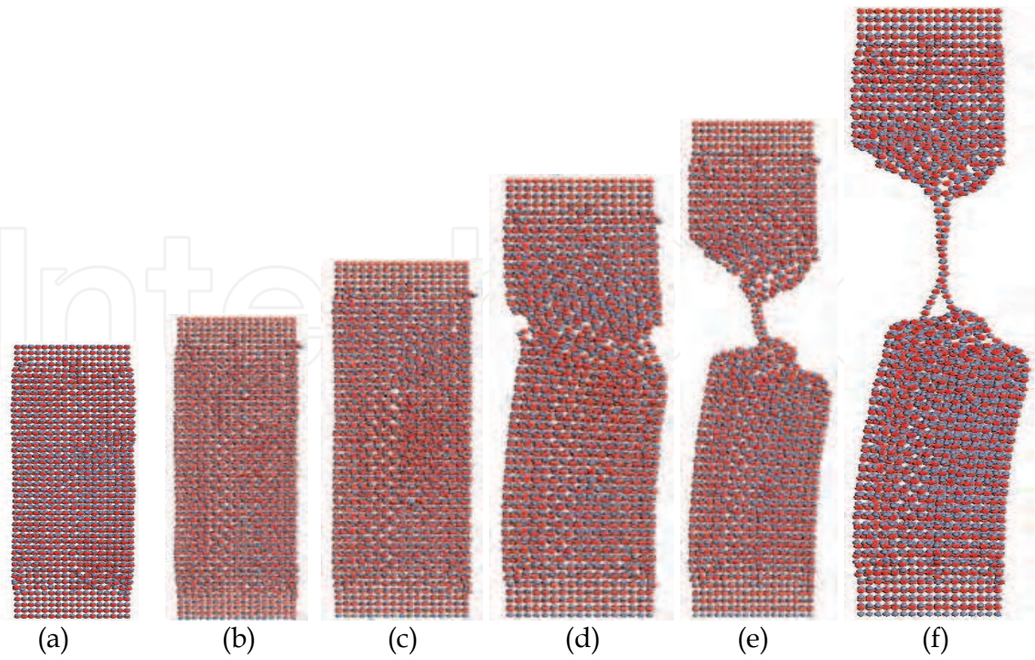

Fig. 3. Tensile stretching of 25Å diameter ZnO nanowire - (a) equilibration, (b) straightening at 12.5% strain, (c) formation of amorphous central section at 13.5% strain, (d) neck initiation at 14.4% strain, (e) neck shrinkage and formation of bi-lines at 38.5% strain, and (f) atomic neck pulling at 57.7% strain.

The displacement history of five atoms in the single-atom-neck chain (Fig.3e) is presented in Fig.4 to describe the deformation process. The five atoms were originally a twisted atomic

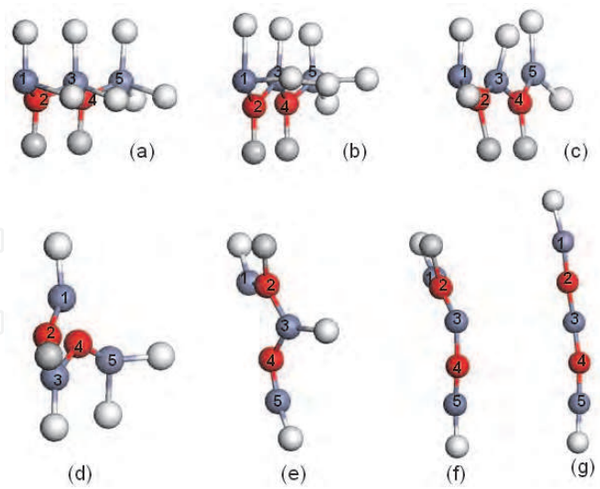

Fig. 4. Deformation process for five atoms within a single-atom-neck chain in Fig.3e. The atoms from which necking initiated are numbered 1 to 5, and the neighboring bonded atoms were shown as light grey dots. The neighbor atoms can be O or Zn atoms, which form ionic bonds with the neck atoms. The deformation process was depicted in seven snapshots (a) original lattice sites, (b) elastic stretch, (c) plastic deformation with bond breakage, (d)-(f) deformation during thining of wire neck, and (f) formation of the single atom chain.

chain on the lattice sites of two adjacent crystals located at the nanowire surface (Fig.4a). At the initial stage of stretching, these atoms were slightly strained (Fig.4b) to take up the axial expansion. Then, bond breakage was observed for atom-3 and 5, and the atomic morphology was significantly deformed (Fig.4c), in accordance with the crystalline–to-amorphization transformation as depicted in Fig.3c. Afterwards, debonding was continuously occurring (Fig.4d-f), and each debonding relaxed the straightened atomic chain before further deformation until the formation the single-atom-neck chain (Fig.4g). This isolated atomic chain was then observed to grow via the addition of more atoms to the head and tail atoms (atoms 1 and 5 initially).

The key for the extreme ductility lies in whether an atom on the wire at the junction of the single atom chain detaches itself from the bulk to join the chain or if the chain breaks first. As shown in Fig.5, at one end of the single atom chain, atom-X is bonded to three atoms - one within the neck chain, and other two on the amorphous bulk. The forces acting on atom-X is expressed in equation-1,

$$N = \sum F_n \cos\theta_n = F_1 \cos\theta_1 + F_2 \cos\theta_2 \tag{1}$$

In equation-1, if the value of cosθ is less than 0.5, force vector $\mathbf{F_i}$ is likely to be higher than $\mathbf{N}$. In the simulation models, the angle θ was measured as 58-74˚, thereby cosθ is most likely to be less than 0.5. This means the bond breakage will likely happen in the bulk, supporting the atomic neck chain to grow. After the bond breakage, atom-X joined the neck chain and the atom in the amorphous bulk that was still bonded to it, became the new connection between the neck chain and the amorphous bulk. The process was continuously repeated during the simulation process, leading to super ductility of the nanowire.

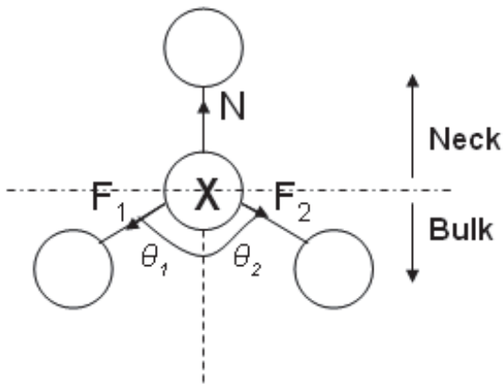

Fig. 5. Forces at the junction between the single-atom-neck chain and the amorphous bulk in the nanowire.

Fig.6 plots the stress-strain curve and change in number of Zn-O bonds (NZB) for the 25Å nanowire. Four regimes - linear (regime A), amorphization (regime B), neck shrinking (regime C) and neck chain growth (regime D) - were defined based on the deformation behavior. It gives a Young's modulus of 203 GPa and ultimate tensile strength of 8.89 GPa. Meanwhile, the 7Å diameter ZnO nanowire was much softer with 48.8 GPa Young's modulus and 2.87 GPa UTS.

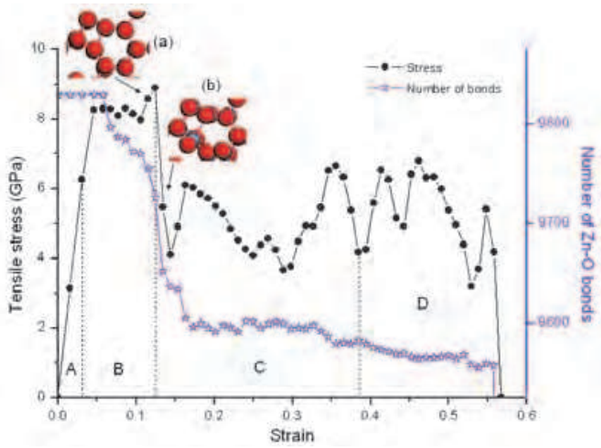

Fig. 6. Curves of tensile stress and number of Zn-O bonds for 25Å nanowire, where four zones were defined as different deformation behavior. Charts (a) and (b) are the regional cross-section views accounting for the crystalline to amorphous transformation via the difference of atomic misfit in their top views.

2.2 TiO_2

TiO_2 nanowires are often studied by experimentalists because they have wide range of applications and are suitable for many experimental techniques(Diebold 2003). Beyond experimental attractions, the theoretical studies have been carried out for analyzing nanocrystal structures, such as nanoparticles(Hallil, Tetot et al. 2006) and nanoclusters (Collins, Smith et al. 1996; Filyukov, Brodskaya et al. 2007). However, there is still a lack of literature on modeling the TiO_2 nanowires to present an overall understanding of the mechanism behind experimental observations.

We use Matsui and Akaogi's potential(Matsui and Akaogi 1991) for the atomic interactions, and MD simulations to study for the tensile deformation of the nanowire(Dai, Tan et al. 2009). The TiO_2 nanowire model was built from the most stable rutile crystal structure with the [100] direction along the wire axis. The nanowire is cylindrical, 59.18 Å in length and 27.6 Å in diameter and contains 3500 atoms. Firstly, the model was dynamically relaxed for 2 ns, resulting in an expansion of about 0.67% in volume, as shown in Fig.7. It can be seen that the equilibration relocated the surface atoms while the core atomic arrangement remained unchanged.

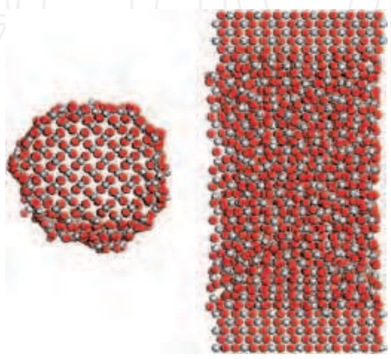

Fig. 7. Top (left) and front (right) view of equilibrated cylindrical TiO_2 nanowire model. The relaxed surface atoms take up about 39.4% of the total free atoms.

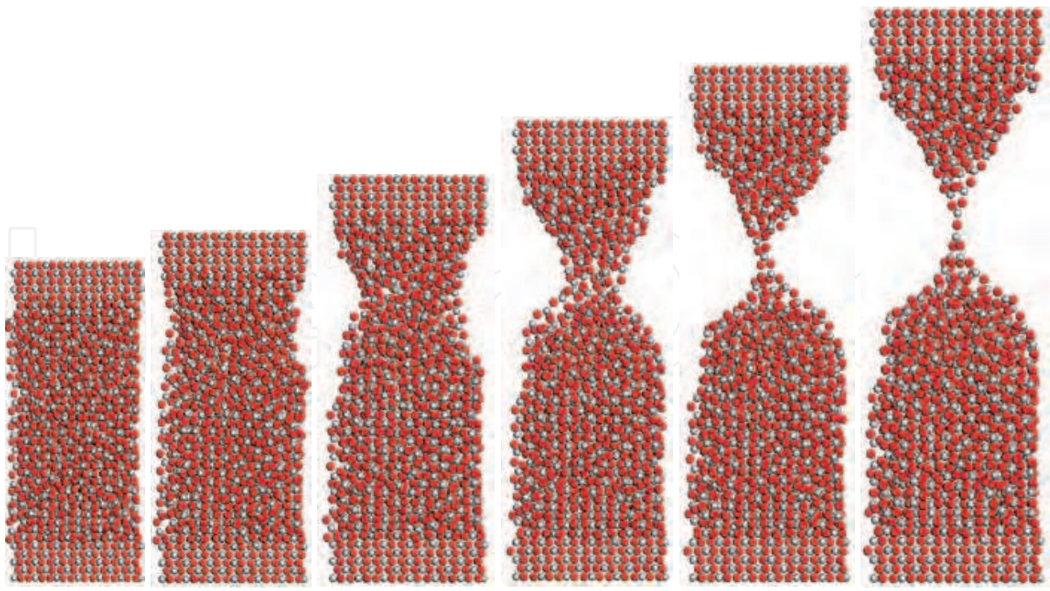

Fig. 8. Tensile process of TiO_2 nanowire at different strain levels - (a) 1.6%, (b) 8.4%, (c) 20%, (d) 35.2%, (e) 43.6% and (f) 53.7%.

The snapshots of tensile process are presented in Fig.8. After a small initial linear stretching, bond breakage appeared at the surface, giving rise to the necking phenomenon. With continuous surface atom bond breaking, new surfaces were created to shrink the neck into single-atom-neck chain. In the single-atom-neck chain structure, it fails to meet the criteria of chain growth (θ <60˚), and soon ruptured.

The tensile deformation of TiO_2 nanowires was dominated by the free surface effect. Fig.9 presents the tensile induced deformation process of a group of surface atoms at five instances, namely, initial equilibration (chart a), yielding (chart b), ultimate tensile stress (UTS) (chart c) and two steps of plastic necking deformation (chart d and e). Plastic deformation was induced by the bond breakage at the surface which propagated inward resulting in new surfaces being created.

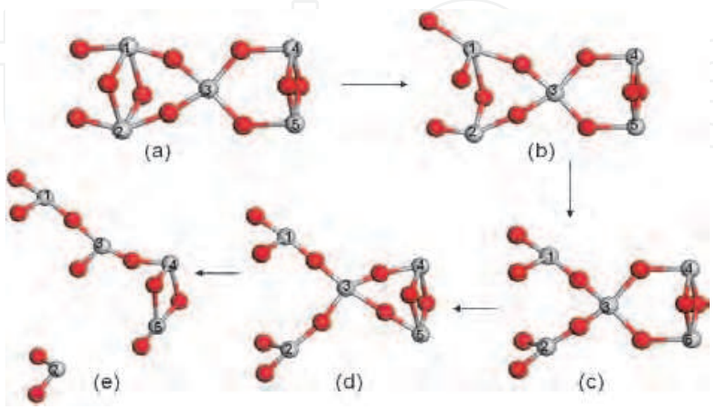

Fig. 9. Atomic re-arrangement during tensile process - (a) initial equilibration, (b) yielding, (c) UTS, (d) necking, (e) further necking. Atoms at the extreme left comprise the side surface whereas atoms 4 and 5 are connected to atoms within the core of the wire.

The bond and stress analysis are shown in Fig.10. Chart (a) shows the stress-strain curve with three additional snapshots of atomic arrangement (I to III) at yielding, UTS, and final single-atom-neck stages, individually. Fig.10 (b)-(d) show the quantative variation of Ti-O bonds, Ti-O bond lengths, and longitudinal projections of Ti-O bond lengths, which reflect the mechanical characteristics.

These charts clearly define the bond-rotation induced elasticity, bond-breakage induced plasticity, and the continuous cycles of bond straightening – bond breakage and inner atomic distortion – neck thinning, beyond UTS until rupture.

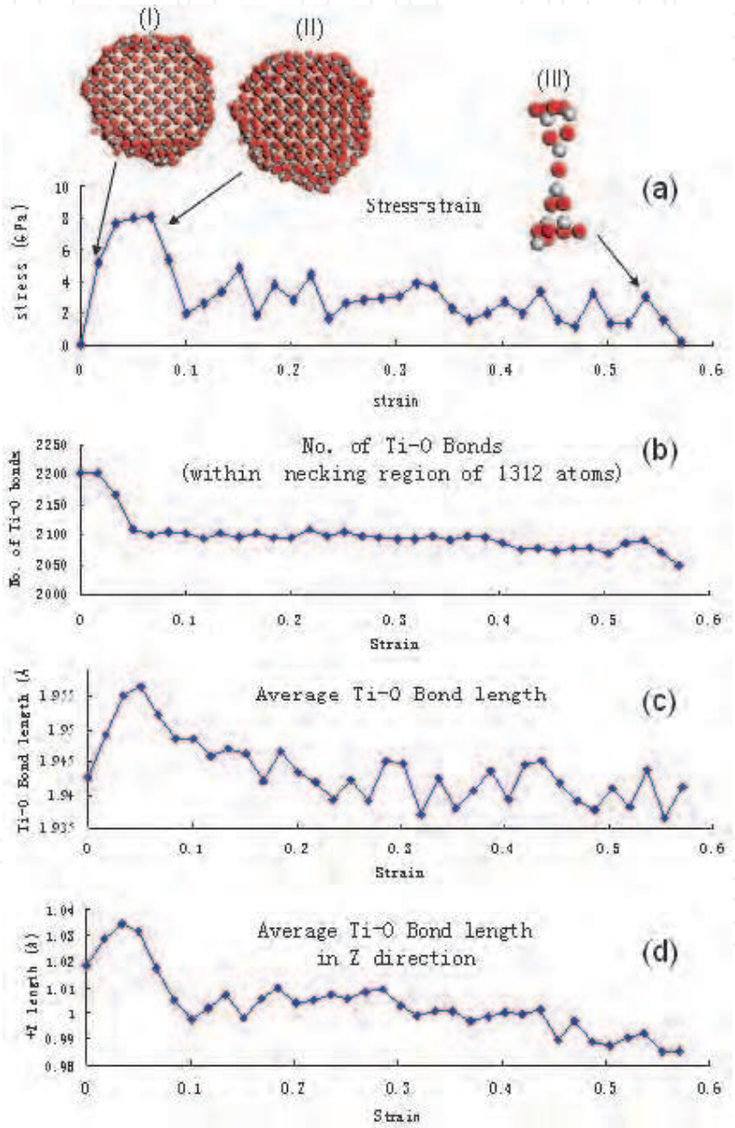

Fig. 10. Data plot of (a) Stress-strain curve (b) Number of Ti-O bonds (c) Average length of Ti-O bonds (d) Average length of Ti-O bonds projected onto the longitudinal direction. Charts (b), (c) and (d) are only for the necking region which includes 1312 atoms. In chart (a), the three insets are cross-sectional atomic arrangements at yielding, just beyond UTS and during single-atom-necking.

More TiO_2 nanowires with different lateral size were used for tensile simulations to investigate the size effect. These TiO_2 nanowires all showed similar deformation processes due to the domination of the surface effect. However, in contrast to the case of ZnO, TiO_2 nanowires showed enhanced stiffness and UTS with decreasing wire thickness as shown in Fig.11. The reason for the different size effects on mechanical property lies in the mechanisms of structural deformation, which will be discussed later in this chapter.

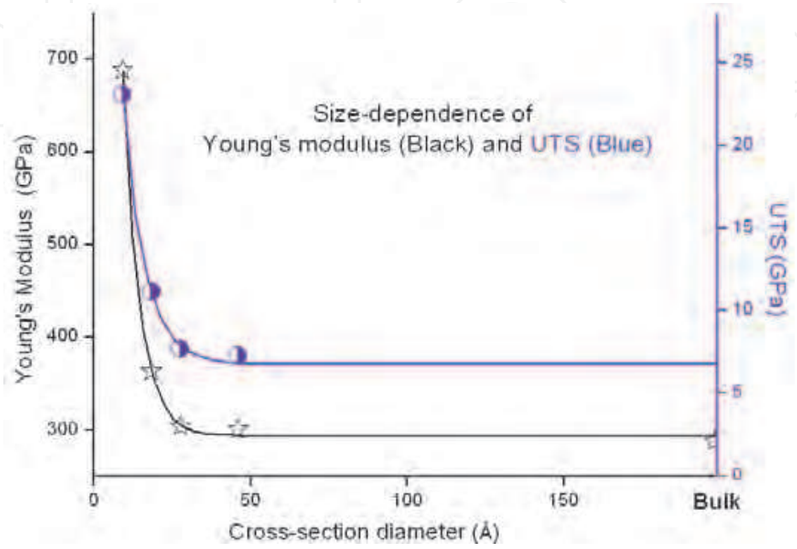

Fig. 11. Young's modulus and UTS as functions of nanowire thickness.

2.3 CuO

CuO plays an important role in building high temperature superconductors, and its nanowire has potential applications as an electron field emission source. Synthesis of CuO nanowires have been reported during the last decade(Wang, Zhan et al. 2001; Jiang, Herricks et al. 2002).

We used AFM and three-point bend test to measure the Young's modulus of nanowire(Tan, Zhu et al. 2007). CuO nanowires were synthesized via vapor-solid pre-action method, and deposited on the AFM calibration grid spanning across the holes, as shown in Fig.12. With one end of the nanowire fixed, a point load of up to 40-90 nN was applied to the other free end by an AFM tip. The Young's modulus could then be calculated from beam bending theory via equation-2.

$$E = \frac{FL^3}{192\delta I} \tag{2}$$

Here, E is the Young's modulus, F is the maximum force applied, L is the suspended length, δ is the deflection of the beam at the mid-span and I is the second moment of area (where $I = \pi D^4/64$ and D is the beam diameter).

The Young's modulus was also calculated theoretically via computing the elastic constants of CuO crystals, and the polycrystalline properties were predicted via Hashin-Shtrikman bound theory(Watt 1980). Good agreement was achieved between experimental and computational values as depicted in Fig.13.

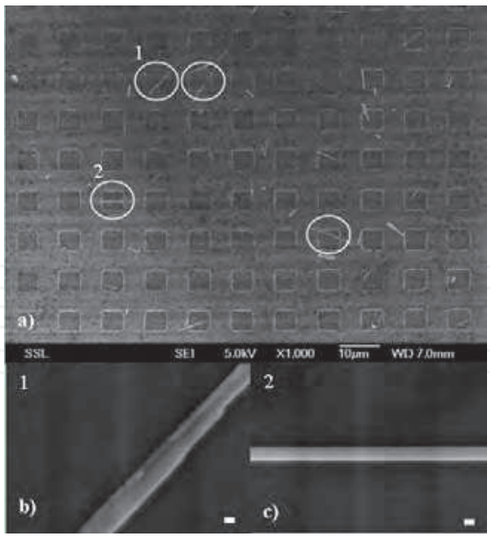

Fig. 12. Scanning electron microscopy images of CuO nanowires deposited on AFM calibration grid. (a) nanowires spanning across holes with two indicated location-1 and 2, (b) close-up image of tapered nanowire at location-1, (c) close-up image of uniform nanowire at location-2.

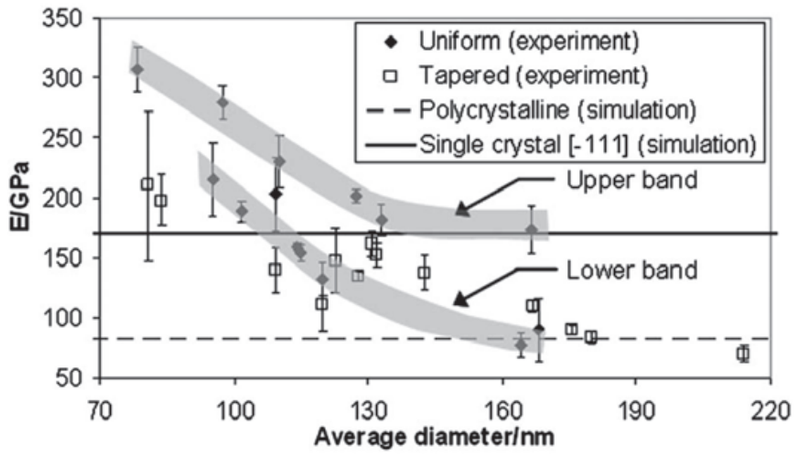

Fig. 13. Variation of Young's modulus with nanowire diameter for uniform and tapered nanowires. Theoretical values for single and polycrystalline CuO crystals are from numerical calculations.

2.4 Co_xO_y

Nanostructured Co_3O_4 has excellent electrochemical reactivity and is important in applications of lithium-ion batteries, gas sensing etc. Synthesis of its crystalline structure(Petitto and Langell 2004) and nanowire(Li, Tan et al. 2006) has been reported.

In our work, the Co_3O_4 nanowires were fabricated by vapor-solid method(Varghese, Teo et al. 2007) and measured via three-point-bend test. Furthermore, some Co_3O_4 nanowires were converted into CoO nanowires via annealing, and tested for the mechanical properties (Fig.14).

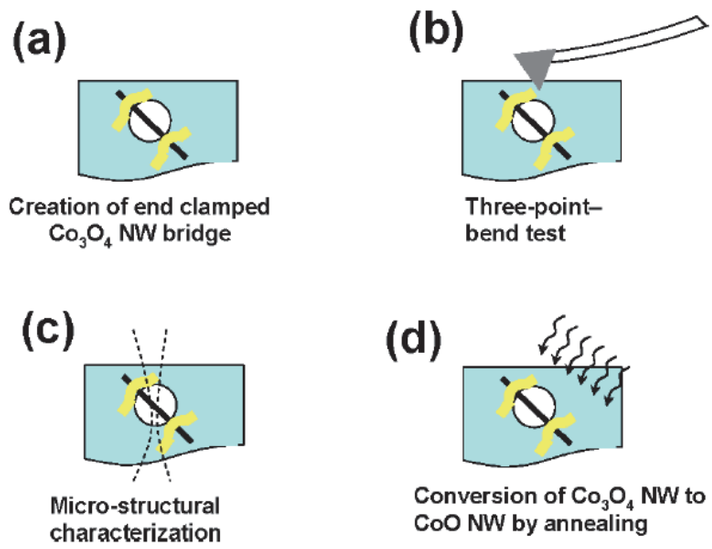

Fig. 14. Schematic of the characterization process for Co_3O_4 and CoO nanowires.

The Young's modulus was also calculated theoretically and compared with our experimental values. Fig.15 clearly shows a trend of weakness with increasing of lateral diameter for Co_3O_4 nanowires. Some thinner samples agree well with theoretical values, but most samples are lower than the polycrystalline value. The reason lies in the defects, impurities, and discontinuities in the specimens, especially significant for the thicker nanowires.

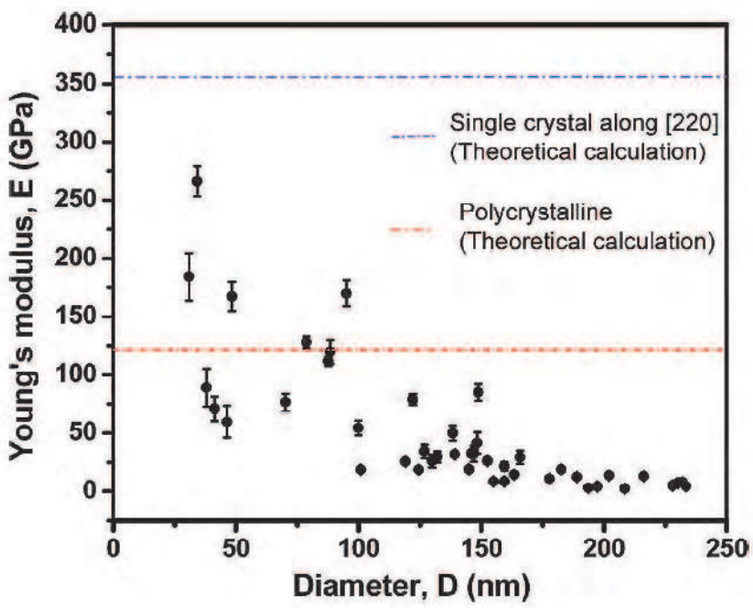

Fig. 15. Young's modulus of Co_3O_4 nanowires vs lateral diameter.

The anneal CoO was also tested and the results are presented in Fig.16. After annealing, these nanowires became more brittle. Thinner nanowires become softer, but thicker ones retained similar stiffness.

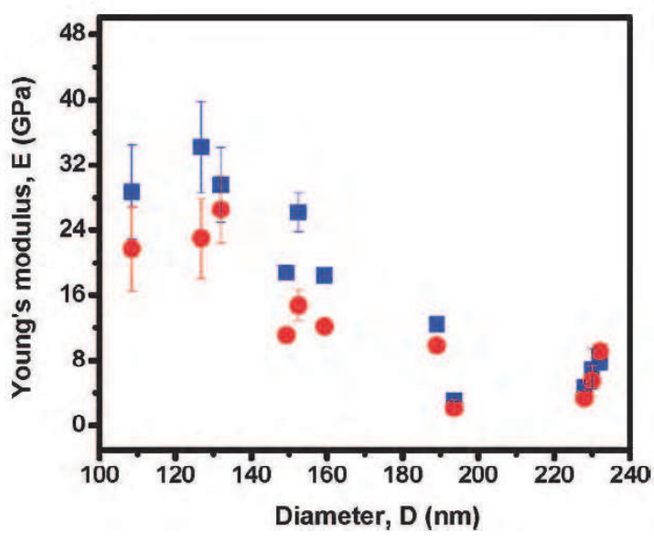

Fig. 16. Young's modulus of CoO nanowires vs lateral diameter. For comparison, the same nanowire before annealing is shown in blue.

2.5 V_2O_5

V_2O_5 exhibits remarkable electrochemical properties and is regarded as an ideal electrode material for Li-based battery(Lu, Chang et al. 2006). Its crystal structure shows highly anisotropic lattice morphology and mechanical stiffness.

In our work, the V_2O_5 polycrystalline nanowires were fabricated via solid-vapor method, and have been measured mechanically through resonance testing(Zhu, Zhang et al. 2010). The results are presented in Fig.17.

The as-grown nanowire was characterized as $V_2O_5 \cdot nH_2O$, where the V_2O_5 crystals were highly randomly arranged. The measured Young's modulus showed a wide distribution from 5.6 up to 98 GPa. The stiff thin nanowires were highly anisotropic and very weak laterally. After annealing at 450°C in vacuum, the nanowires were converted into polycrystalline α-V_2O_5 phase, with Young' modulus averaging around 29 GPa.

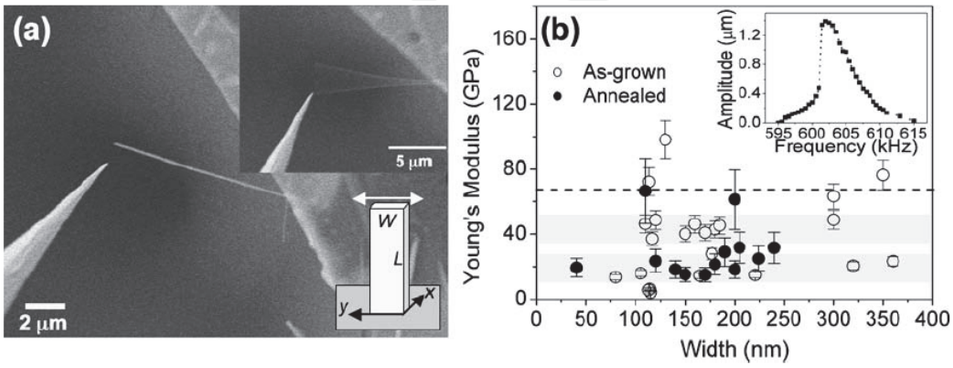

Fig. 17. (a) SEM image of a $V_2O_5 \cdot nH_2O$ nanowire, with insets showing the image of the same nanowire under resonance (upper) and schematic vibration along the width direction. (b) Young's modulus of as-grown and annealed nanowires, with dotted lines indicating the theoretical value; the inset is a typical resonance peak.

Tensile simulation of molecular dynamics was also carried out for V_2O_5 nanowires. Similar to the case of TiO_2, the deformation process was strongly dominated by the free surface effect, and resulted in brittle rupture with short single-atom-neck chain. The Young's modulus was measured to be 116 GPa, and UTS was calculated as 3.8 GPa.

2.6 WO_3

Tungsten trioxide (WO_3) has been extensively studied because of its extraordinary electrochromic, ferroelectric and semiconductor properties (Woodward, Sleight et al. 1995; Lugovskaya, Aleshina et al. 2002; Lu, Chen et al. 2007).

We synthesized WO_{3-x} (with some oxygen starvation defects) nanowires by means of solid-vapor method(Cheong, Varghese et al. 2007). Well aligned nanowires were observed as shown in Fig.18.

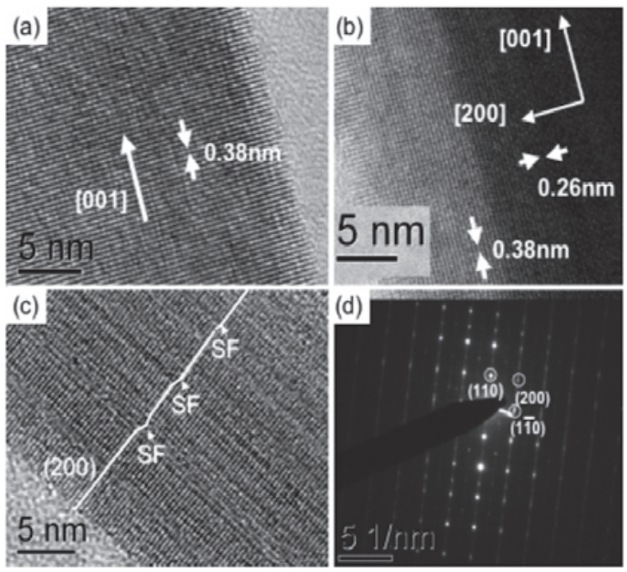

Fig. 18. HRTEM images of (a) WO_{3-x} nanowire; (b) a nanowire showing (001) and (200) lattice spacing; (c) a segment of nanowire with stacking fault ('SF' in the image) at (200) plane; (d) Electron diffraction image of a single nanowire.

From three-point bend tests, the Young's modulus of the nanowires was measured to be 10-100 GPa, lower than the theoretical perfect crystalline values of 310 GPa due to the existence of defects. Furthermore, these nanowires were found to be good field emitters with a field enhancement factor estimated to be $9.8*10^4$ cm^{-1}.

2.7 Other oxides

The reported structure-mechanical investigations for metal oxide nanowires have been very limited. Apart from Kukarni's work on ZnO nanowires(Kulkarni, Zhou et al. 2005; Kulkarni and Zhou 2006; Wang, Kulkarni et al. 2008), MgO nanowires were reported by Xiong et al. arising molecular dynamics simulations. It was found that the MgO nanowires appear more ductile at low strain rates, and the tensile strength decreases as the cross-sectional diameter decreases or temperature increases. However, the applied strain rates of 25 and 100 m/s may have resulted in very stiff and brittle mechanical response.

A series of metal oxide nanowires (MgO, Fe_2O_3, MnO) together with previously mentioned ZnO, TiO_2 and V_2O_5, under tension have been simulated. Two different types of deformation processes were observed. For ZnO, MgO and MnO nanowires, the atomic bonds are highly flexible and can rotate easily. These gave rise to super ductility of the nanowire. On the other hand, the deformation of nanowires of TiO_2, V_2O_5 and Fe_2O_3 are dominated by free surface effect which resulted in brittle fracture. All the ultra thin nanowires (lateral diameter <10Å) showed similar surface effects under tensile loading, but the ductility remained unchanged above a certain thickness.
From their stress-strain curves, the Young's moduli and UTS were obtained, and compared with theoretical polycrystalline calculations and experimental measurements, as presented in Table-1. It can be seen that the Young's modulus agree very well among the three sources of data. However, the simulation results for UTS are much higher than experimental values due to the existence of various defects in the samples.

Material	Young's modulus (GPa)			UTS (GPa)	
	Simulation	Bulk	Experiment	Simulation	Experiment
MgO	309	294(Watt 1987)	246.7(Samsonv 1982)	6.33	0.98(Samsonv 1982)
MnO	128.3	108.4(Watt 1987)	-	5.05	-
ZnO	202	140(Watt and Peselnick 1980)	100-220(Dai, Cheong et al. 2010)	8.89	2.5-7.5(Dai, Cheong et al. 2010)
TiO2	304	277(Watt 1986)	287.9(Isaak, Garnes et al. 1998)	8.15	0.054-0.068(Samsonv 1982)
Fe2O3	148.7	142.5(Watt and Peselnick 1980)	-	7.25	-
V2O5	116	68.1(Watt 1979)	-	3.8	-

Table 1. Mechanical properties of the nanowires that equilibrated with crystalline cores.

3. Discussion

The different mechanical responses of above mentioned metal oxide nanowires were analyzed and found to be structure related.
Fig.19 describes the atomic trajectories of six atoms that were originally located in a lateral surface of a ZnO type nanowire. It shows that the plastic deformation process was originally induced with evenly distributed longitudinal tensile bond forces, and caused selective longitude bond breaking and out-of-plain distortion of atomic planes, finally giving rise to a configuration that supports the growth of atomic neck chain and consequently leading to super ductility.

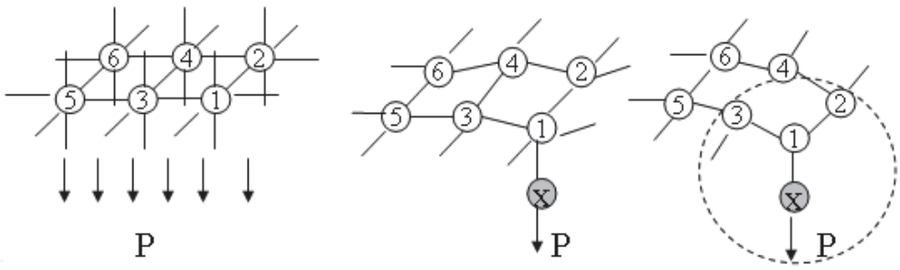

Fig. 19. Process of atomic deformation of ZnO type nanowires, from plane cleavage, plane deformation to atomic chain growth. The atomic arrangement withing the dash circled region determines if a single atom chain will grow or break according to equation-1.

On the other hand, the crystal structure of TiO_2 type materials shows a lower symmetry of atomic distribution lattice, leading to anisotropic deformations when stress is applied. In Fig.20, which shows the displacement history of atoms originally located on a lateral surface, it is observed that bond stretching and breakage initiate from the surface (atoms 1, 4, 6 and 8 are on the surface) and propagate to the inner core. The atomic neck chain was formed at the stage shown in Fig.20c. However, the criterion for single atom chain growth of equation-1 was not satisfied and the nanowire soon ruptured.

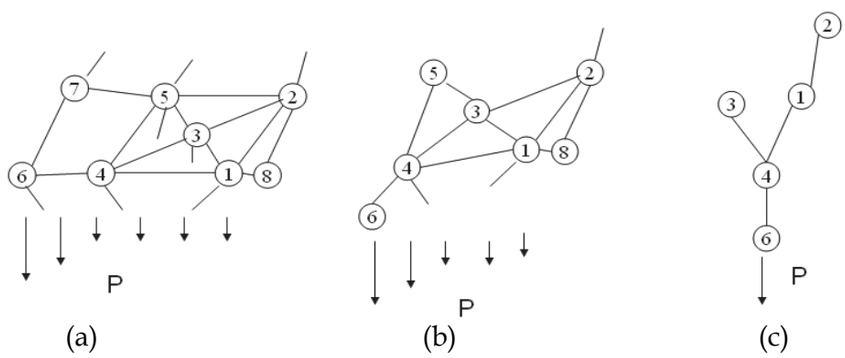

Fig. 20. Atomic deformation of TiO_2 type nanowires, showing a concentration of bond forces at the surface.

The stress-strain curves are presented in Fig.21. All the nanowires have similar trend in their stress-strain curves - the tensile stress jumps sharply during the elastic stage and soon reaches the ultimate tensile stress (UTS). Beyond UTS, the stresses oscillated about a considerably lower value. The tensile process reaches over 100% strain for ZnO type nanowires, but ends with rupture at around 20%-60% strain for TiO_2 type nanowires.
Significant differences were also predicted for how wire diameter affected the two groups of nanowires. The tensile stress was quite low for ultra thin ZnO type nanowires, and the mechanical response gradually enhanced to bulk values with size increase whereas an opposite mechanical trend of size effect was observed for TiO_2 type nanowires which showed that ultra thin nanowires possess superior mechanical properties. As depicted in Fig.19 and Fig.20, the atomic bonds in ZnO type structure are more flexible and are more able to rotate to accommodate the tensile stretching, whereas in TiO_2 type structure, tensile deformation was effected increasingly through the stretching of individual bonds as the nanowires decrease in size.

The key feature determining the difference in the mechanical behaviors between the two types of metal oxide nanowires lies in whether continuous and highly symmetrical atomic surface of the metal oxide polycrystals are formed. With a symmetrical structure, super tensile ductility can be expected. The characteristics of the two types are considered to be representative of metal oxide nanowires. Due to the large number and complex compositions of various metal oxides, there may be other structure and property characteristics that require further investigation.

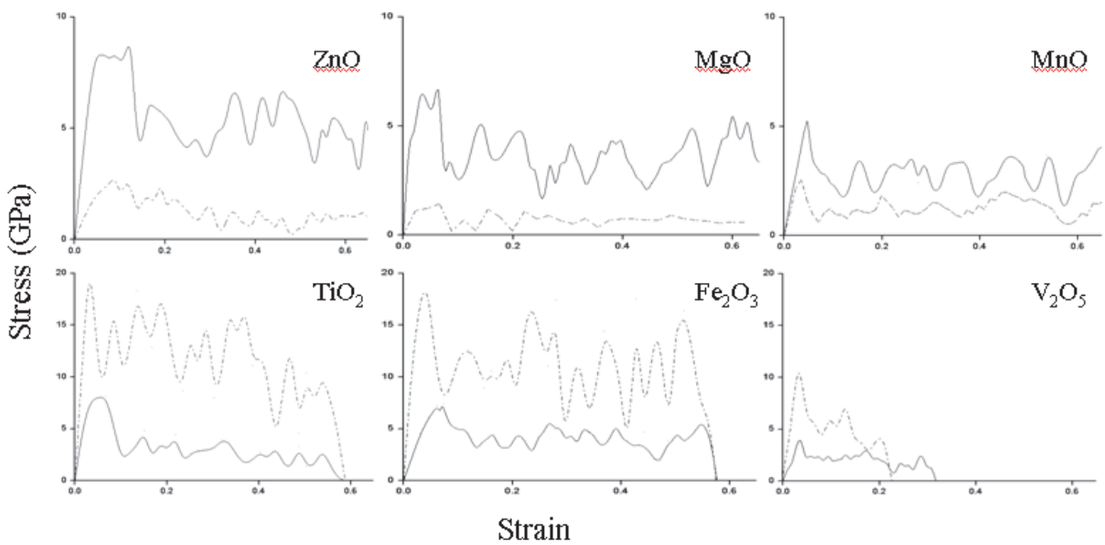

Fig. 21. Stress-strain curves for the six types of nanowire with different lateral size. Solid lines are for the nanowires of around 25 Å lateral diameter and dashed lines for the ultra thin nanowires of around 8 Å lateral diameter.

4. Conclusion

In conclusion, we have reviewed published literature on the structure and mechanical properties of metal oxide nanowires. Due to their unique properties, metal oxide nanowires have been widely considered to play an important role in the next generation of materials. It is a clear trend that the experiment and simulation research activities will need to complement one another to understand their structure-mechanical property relations for the successful application of nanowires.

The development of experimental characterization and numerical simulation occurs in tandem. Simulation reveals the mechanism and predicts actual phenomena, which can help to direct the experimental process, saving time and cost. On the other hand, experimental characterizations can provide calibration data to improve the efficiency and effectiveness of simulation works.

5. Acknowledgment

This work is supported by the funding from the Science and Engineering Research Cuncil (SERC, A*STAR) and Institute of Mterials Research and Engineering (IMRE, A*STAR), Singapore.

6. References

Agrawal, R., B. Peng, et al. (2008). "Elasticity Size Effects in ZnO Nanowires-A Combined Experimental-Computational Approach." Nano Lett. 8: 3668.

Bai, X. D., P. X. Gao, et al. (2003). "Dual-mode mechanical resonance of individual ZnO nanobelts." Appl. Phys. Lett. 82: 4806.

Chen, C. Q., Y. Shi, et al. (2006). "Size Dependence of Young's Modulus in ZnO Nanowires." Phys. Rev. Lett. 96: 075505.

Chen, X., S. M. Sun, et al. (2002). "Self-Assembling Vanadium Oxide Nanotubes by Organic Molecular Templates." Inorg. Chem. 41: 4524.

Cheong, F. C., B. Varghese, et al. (2007). "WO3-x nanorods synthesized on a thermal hot plate." J. Phys. Chem. C 111: 17193.

Collins, D. R., W. Smith, et al. (1996). "Molecular dynamics study of Ti02 microclusters." J. Mater. Chem 6: 1385.

Dai, L., W. C. D. Cheong, et al. (2010). "Molecular Dynamics Simulation of ZnO Nanowires – Size Effects, Defects and Super Ductility." Langmuir 26: 1165.

Dai, L., V. B. C. Tan, et al. (2009). "Numerical Investigations into the Tensile Behavior of TiO2 Nanowires : Structural Deformation, Mechanical Properties and Size Effects." Nano Lett. 9: 576.

Dai, Z. R., Z. W. Pan, et al. (2001). "Ultra-long single crystalline nanoribbons of tin oxide." Solid State Comm. 118: 351.

Desai, A. V. and M. A. Haque (2007). "Mechanical properties of ZnO nanowires." Sensors and Acutators A 134: 169.

Diebold, U. (2003). "The surface science of titanium dioxide." Surf. Sci. Reports 48: 53.

Feng, G., W. D. Nix, et al. (2006). "A study of the mechanical properties of nanowires using nanoindentation." J. Appl. Phys. 99: 074304.

Filyukov, D. V., E. N. Brodskaya, et al. (2007). "Molecular-Dynamics Simulation of Nanoclusters of Crystal Modifications of Titanium Dioxide." Russ. J. Gen. Chem. 77: 10.

Gulseren, O., F. Ercolessi, et al. (1998). "Noncrystalline Structures of Ultrathin Unsupported Nanowires." Phys. Rev. Lett. 17: 3775.

Guo, L., Z. H. Wu, et al. (2000). "Synthesis of novel Sb O and Sb O nanorods." Chem. Phys. Lett. 318: 49.

Hallil, A., R. Tetot, et al. (2006). "Use of a variable-charge interatomic potential for atomistic simulations of bulk, oxygen vacancies, and surfaces of rutile TiO_2." Phys. Rev. B 73: 165406.

Heo, Y. W., D. P. Norton, et al. (2004). "ZnO nanowire growth and devices." Mater. Sci. Eng. R 47: 1.

Hoffmann, S., F. Ostlund, et al. (2007). "Fracture strength and Young's modulus of ZnO nanowires." Nanotechnology 18: 205503.

http://www.cse.scitech.ac.uk/ccg/software/DL_POLY/.

Huang, Y. H., X. D. Bai, et al. (2006). "In situ mechanical properties of individual ZnO nanowires and the mass measurement of nanoparticles." J. Phys.: Condens. Matter 18.

Isaak, D. G., J. D. Garnes, et al. (1998). "Elasticity of TiO2 rutile to 1800 K." Phys. Chem. Minerals 26: 31.

Jiang, X. C., T. Herricks, et al. (2002). "CuO Nanowires Can Be Synthesized by Heating Copper Substrates in Air." Nano Lett. 2: 1333.

Kondo, Y. and K. takayanagi (2000). "Synthesis and Characterization of Helical Multi-Shell Gold Nanowires." science 289: 606.

Kulkarni, A. J. and M. Zhou (2006). "Size-dependent thermal conductivity of zinc oxide nanobelts." Appl. Phys. Lett. 88.
Kulkarni, A. J., M. Zhou, et al. (2005). "Orientation and size dependence of the elastic properties of zinc oxide nanobelts." Nanotechnology 16: 2749.
Lakshmi, B. B., C. J. Partissi, et al. (1997). "Sol-Gel Template Synthesis of Semiconductor Oxide Micro- and Nanostructures." Chem. Mater. 9: 2544.
Law, M., J. Goldberger, et al. (2004). "Semiconductor Nanowires and Nanotubes." Annu. Rev. Mater. Res. 34: 83.
Li, C., D. H. Zhang, et al. (2003). "Diameter-controlled growth of single-crystalline IN2O3 nanowires and their electronic properties." Adv. Mater. 2: 143.
Li, D. and Y. N. Xia (2003). "Fabrication of Titania Nanofibers by Electrospinning." Nano Lett. 3: 555.
Li, G. L. and G. H. Wang (1999). "Synthesis and characterization of rutile TiO2 nanowhiskers." J. Mater. Res. 14: 3346.
Li, Y. G., B. Tan, et al. (2006). "Freestanding Mesoporous Quasi-Single-Crystalline Co3O4 Nanowire Arrays." J. Am. Chem. Soc. 128: 14258.
Lu, D. Y., J. Chen, et al. (2007). "Raman study of thermochromic phase transition." Appl. Phys. Lett. 90.
Lu, J. G., P. C. Chang, et al. (2006). "Quasi-one-dimensional metal oxide materials—Synthesis, properties and applications." Mater. Sci. Eng. R 52: 49.
Lu, W. and C. M. Lieber (2006). "Semiconductor nanowires." J. Phys. D: Appl. Phys. 39: R387.
Lugovskaya, L. A., L. A. Aleshina, et al. (2002). "X-ray study and structure simulation of amorphous tungsten oxide." Acta Crystallofr. Sec. B 58: 576-586.
Ma, R. Z. and Y. S. Bando (2003). "Uniform MgO nanobelts formed from in situ Mg3N2 precursor." Chem. Phys. Lett. 370: 770.
Maleev, M. A., D. Srivastava, et al. (2006). "Silicon carbide nanowires under external loads: An atomistic simulation study." Phys. Rev. B 74: 165303.
Manoharan, M. P., A. V. Desai, et al. (2008). "Synthesis and Elastic Characterization of Zinc Oxide Nanowires." J. Nanomater. 2008: 1.
Matsui, M. and M. Akaogi (1991). "Molecular dynamics simulation of the structural and physical properties of the four polymorphs of TiO_2." Mol. Sim. 6(4): 239.
Ni, H. and X. D. Li (2006). "Young's modulus of ZnO nanobelts measured using atomic force microscopy and nanoindentation techniques." Nanotechnology 17: 3591.
Petitto, S. C. and M. A. Langell (2004). "Surface composition and structure of Co_3O_4(110) and the effect of impurity segregation." J. Vac. Sci. Technol. A 22: 1690.
Rao, C. N. R., F. L. Deepak, et al. (2003). "Inorganic nanowires." Prog. Solid State Chem. 31: 5-147.
Samsonv, G. V. (1982). The Oxide Handbook. New York - Washington - London.
Shankar, K. S. and A. K. Raychaudhuri (2005). "Fabrication of nanowires of multicomponent oxides: Review of recent advances." Mater. Sci. Eng. C 25: 738.
Song, J. H., X. D. Wang, et al. (2005). "Elastic Property of Vertically Aligned Nanowires." Nano Lett. 5: 1954.
Tan, E. P. S., Y. Zhu, et al. (2007). "Crystallinity and surface effects on Young's modulus of CuO nanowires." Appl. Phys. Lett. 90: 163112.
Tian, Z. R., J. A. Voigt, et al. (2003). "Complex and oriented ZnO nanostructures." Nature Mater. 2: 821.
Urban, J. J., J. E. Spanier, et al. (2003). "Single-crystalline Barium Titanate Nanowires." Adv. Mater. 15: 423.

Valcarcel, V., A. Souto, et al. (1998). "Development of Single-Crystal a-Al2O3 Fibers by Vapor-Liquid-Solid Deposition (VLS) from Aluminum and Powdered Silica." Adv. Mater. 10: 138.
Varghese, B., C. H. Teo, et al. (2007). "Co3O4 Nanostructures with Different Morphologies and their Field-Emission Properties." Adv. Funct. Mater. 17: 1932.
Vayssieres, L. (2003). "Growth of arrayed nanorods and nanowires of ZnO from aqueous solutions." Adv. Mater. 15: 464.
Wang, B. L., S. Y. Yin, et al. (2001). "Novel Structures and Properties of Gold Nanowires." Phys. Rev. Lett. 86: 2046.
Wang, B. L., S. Y. Yin, et al. (2001). "Structures and electronic properties of ultrathin titanium nanowires." J. Phys.: Condens. Matter 13: L403.
Wang, J., A. J. Kulkarni, et al. (2008). "Novel mechanical behavior of ZnO nanorods." Comput. Methods Appl. Mech. Engrg. 197: 3182.
Wang, W. Z., Y. J. Zhan, et al. (2001). "One-step, solid-state reaction to the synthesis of copper oxide nanorods in the presence of a suitable surfactant." Chem. Comm.: 727.
Wang, X. D., J. H. Song, et al. (2007). "Nanowire and nanobelt arrays of zinc oxide from synthesis to properties and to novel devices." J. Mater. Chem 17: 711.
Watt, J. P. (1979). "Hashin-Shtrikman bounds on the effective elastic moduli of polycrystals with orthorhombic symmetry." J. Appl. Phys. 50: 6290.
Watt, J. P. (1980). "Hashin-Shtrikman bounds on the effective elastic moduli of polycrystals with monoclinic symmetry." J. Appl. Phys. 51: 1520.
Watt, J. P. (1986). "Hashin-Shtrikman bounds on the effective elastic moduli of polycrystals with trigonal(3,-3) and tetragonal(4,-4,4m) symmetry." J. Appl. Phys. 60: 3120.
Watt, J. P. (1987). "POLYXSTAL: A FORTRAN PROGRAM TO CALCULATE AVERAGE ELASTIC PROPERTIES OF MINERALS FROM SINGLE-CRYSTAL." Comput. Geosci. 13: 441.
Watt, J. P. and L. Peselnick (1980). "Clarification of the Hashin-Shtrikman bounds on the effective elastic moduli of polycrystals with hexagonal, trigonal and tetragonal symmetries." J. Appl. Phys. 51: 1525.
Wen, B. M., J. E. Sader, et al. (2008). "Mechanical Properties of ZnO Nanowires." Phys. Rev. Lett. 101: 175502.
Woodward, P. M., A. W. Sleight, et al. (1995). "Structure Refinenment of Triclinic Tungsten Trioxide." J. Phys. Chem. Solids 56: 1305.
Wu, J. M., H. C. Shih, et al. (2006). "Formation and photoluminescence of single-crystalline rutile TiO2 nanowires synthesized by thermal evaporation." Nanotechnology 17: 105.
Wu, J. M., H. C. Shih, et al. (2005). "Thermal evaporation growth and the luminescence property of TiO2 nanowires." J. Cryst. Grow. 281: 384.
Wu, X. C., W. H. Song, et al. (2000). "Crystalline gallium oxide nanowires: intensive blue light emitters." Chem. Phys. Lett. 328: 5.
Xiao, Z. L., C. Y. Han, et al. (2002). "Fabrication of Alumina Nanotubes and Nanowires by Etching Porous Alumina Membranes." Nano Lett. 2: 1293.
Yang, P. D., Y. Y. Wu, et al. (2002). "Inorganic semiconductor nanowires." Int. J. Nanosci. 1(1): 1.
Yum, K. S., Z. Y. Wang, et al. (2004). "Experimental measurement and model analysis of damping effect in nanoscale mechanical beam resonators in air." J. Appl. Phys. 96: 3933.
Zhou, J., C. S. Lao, et al. (2006). "Nanowire as pico-gram balance at workplace atmosphere." Solid State Comm. 139: 222.
Zhu, Y. W., Y. S. Zhang, et al. (2010). "Hotplate Synthesis and Mechanical Characterization of Vanadium Oxide Nanobelts." Acta Mater. 58: 415.

Nanowires - Fundamental Research

Edited by Dr. Abbass Hashim

ISBN 978-953-307-327-9
Hard cover, 552 pages
Publisher InTech
Published online 19, July, 2011
Published in print edition July, 2011

Understanding and building up the foundation of nanowire concept is a high requirement and a bridge to new technologies. Any attempt in such direction is considered as one step forward in the challenge of advanced nanotechnology. In the last few years, InTech scientific publisher has been taking the initiative of helping worldwide scientists to share and improve the methods and the nanowire technology. This book is one of InTechâ€™s attempts to contribute to the promotion of this technology.

How to reference

In order to correctly reference this scholarly work, feel free to copy and paste the following:

L. Dai, C.H. Sow, C.T. Lim and V.B.C. Tan (2011). Metal Oxide Nanowires – Structural and Mechanical Properties, Nanowires - Fundamental Research, Dr. Abbass Hashim (Ed.), ISBN: 978-953-307-327-9, InTech, Available from: http://www.intechopen.com/books/nanowires-fundamental-research/metal-oxide-nanowires-structural-and-mechanical-properties

INTECH
open science | open minds

InTech Europe
University Campus STeP Ri
Slavka Krautzeka 83/A
51000 Rijeka, Croatia
Phone: +385 (51) 770 447
Fax: +385 (51) 686 166
www.intechopen.com

InTech China
Unit 405, Office Block, Hotel Equatorial Shanghai
No.65, Yan An Road (West), Shanghai, 200040, China
中国上海市延安西路65号上海国际贵都大饭店办公楼405单元
Phone: +86-21-62489820
Fax: +86-21-62489821

IntechOpen